


Article

Toxic Effect of Fullerene and Its Derivatives upon the Transmembrane β_2 -Adrenergic Receptors

Longlong Ren ¹, Zhenxiang Jing ¹, Fei Xia ², John Zenghui Zhang ²  and Yang Li ^{3,*}

¹ College of Mechanical and Electronic Engineering, Shandong Agricultural University, Tai'an 271018, China; renlonglong@sdau.edu.cn (L.R.); lyzhenxiangjing@163.com (Z.J.)

² NYU-ECNU Center for Computational Chemistry at NYU Shanghai, School of Chemistry and Molecular Engineering, East China Normal University, Shanghai 200062, China; fxia@chem.ecnu.edu.cn (F.X.); zhzhang@phy.ecnu.edu.cn (J.Z.Z.)

³ College of Information Science and Engineering, Shandong Agricultural University, Tai'an 271018, China

* Correspondence: yang.li@sdau.edu.cn

Abstract: Numerous experiments have revealed that fullerene (C_{60}) and its derivatives can bind to proteins and affect their biological functions. In this study, we explored the interaction between fullerene and the β_2 -adrenergic receptor (β_2AR). The MD simulation results show that fullerene binds with the extracellular loop 2 (ECL2) and intracellular loop 2 (ICL2) of β_2AR through hydrophobic interactions and π - π stacking interactions. In the C_{60} _in1 trajectory, due to the π - π stacking interactions of fullerene molecules with PHE and PRO residues on ICL2, ICL2 completely flipped towards the fullerene direction and the fullerene moved slowly into the lipid membrane. When five fullerene molecules were placed on the extracellular side, they preferred to stack into a stable fullerene cluster (a deformed tetrahedral aggregate), and had almost no effect on the structure of β_2AR . The hydroxyl groups of fullerene derivatives ($C_{60}(OH)_X$, X represents the number of hydroxyl groups, X = 4, 8) can form strong hydrogen bonds with the ECL2, helix6, and helix7 of β_2AR . The hydroxyl groups firmly grasp the β_2AR receptor like several claws, blocking the binding entry of ligands. The simulation results show that fullerene and fullerene derivatives may have a significant effect on the local structure of β_2AR , especially the distortion of helix4, but bring about no great changes within the overall structure. It was found that C_{60} did not compete with ligands for binding sites, but blocked the ligands' entry into the pocket channel. All the above observations suggest that fullerene and its derivatives exhibit certain cytotoxicity.

Keywords: MD simulation; fullerene derivatives; cytotoxicity; β_2 -adrenergic receptor



Citation: Ren, L.; Jing, Z.; Xia, F.; Zhang, J.Z.; Li, Y. Toxic Effect of Fullerene and Its Derivatives upon the Transmembrane β_2 -Adrenergic Receptors. *Molecules* **2022**, *27*, 4562. <https://doi.org/10.3390/molecules27144562>

Academic Editors: Jianzhong Chen, Zhaoxi Sun, Ya Gao and Angelina Angelova

Received: 19 May 2022

Accepted: 10 July 2022

Published: 18 July 2022

Publisher's Note: MDPI stays neutral with regard to jurisdictional claims in published maps and institutional affiliations.



Copyright: © 2022 by the authors. Licensee MDPI, Basel, Switzerland. This article is an open access article distributed under the terms and conditions of the Creative Commons Attribution (CC BY) license (<https://creativecommons.org/licenses/by/4.0/>).

1. Introduction

Since the discovery of fullerene (C_{60}), its functions have attracted the intensive interests of scientists [1,2]. Because of the excellent physical and chemical properties of fullerene, it has become one of the most promising nanomaterials, and has been widely used in the pharmaceutical industry [3–6]. In vivo, fullerene molecules show a tendency to aggregate into nanoparticles which can cross the cell membranes of brains due to their lipophilic properties. Thus, fullerene has been used for drug delivery in vivo because of its high stability and hollow cage-like structure [7,8]. For instance, the diameter of fullerene is comparable to the size of active centers of some viruses, such as HIV, so that it has been utilized to block the entrances of active viral centers and prevent the viruses obtaining nutrition from cells [9–11]. Recently, it has been found that nanomaterials composed of fullerene derivatives could stabilize immune effector cells to inhibit the release of proinflammatory mediators, making them potential candidates for treatment of several diseases including asthma, arthritis and multiple sclerosis [12–16].

In addition to the broad applications of fullerene and its derivatives in the pharmaceutical industry, their potential toxicity also drawn the attention of researchers [17,18]. The

exposure of largemouth bass to nC₆₀ led to lipid peroxidation in the brain and glutathione depletion in their gills, affecting the signal transmission and normal expression of proteins [19,20]. Further experimental studies reported that fullerene nanoparticles destroyed the permeability and integrity of cell membranes as they crossed them [21–24]. Cell membranes are composed of various lipids and transmembrane proteins responsible for the functions and activities of cells. When the fullerene nanoparticles cross the cell membranes, they not only affect the structures and functions of the lipid membranes, but also the transmembrane proteins. Previous experimental studies also revealed that fullerenes could affect the activity and function of proteins, including potassium channel proteins [25,26], HIV proteases [9–11,27,28], serum albumins [29–31] and glutathione *S*-transferases [32–34].

Using microsecond molecular dynamics (MD) simulations, Monticelli et al. investigated the interaction of C₇₀ fullerene with Kv1.2 potassium channel proteins. Their simulated results revealed that the fullerenes acted as blockers to change the conformations and functions of the secondary structures of Kv1.2 [35]. Further MD simulations of fullerenes and their related derivatives indicated that they could bind to hydrophobic sites on the surfaces of proteins through specific interactions such as π - π stacking [36,37]. It is generally understood that such kind of π - π stacking interactions exist between the conjugated surface of C₆₀ and the hydrophobic residues of PHE, TRP, and TYR with aromatic rings.

Fullerene and its derivatives worked as competitors to the ligands of target proteins. Kraszewski et al. found that extracellular fullerene molecules blocked the entry of potassium channel proteins and prevented potassium ions from entering the channel. The intracellular fullerene molecules could enter the channel from the side of the cytoplasm and become stuck in the cavity formed by a few helices of channel protein [25,35]. A series of experimental studies about the cytotoxicity of fullerene derivative C₆₀(OH)_n have also been reported [38–40]. Although there has been a great deal of evidence for the toxicity of fullerene and its derivatives, the atomistic interaction details of fullerenes and related proteins remain unclear so far.

In this study, we performed MD simulation to investigate the toxic effect of fullerenes and their hydroxyl derivatives on the β_2 -adrenergic receptor (β_2 AR), which serves as an important target for cardiac and asthma drugs, and is an extensively studied model system within the G-protein coupled receptor (GPCR). β_2 AR is the protein that mediates muscle relaxation in bronchi, as well as vasoconstriction and vasodilation, the structure of which is shown in Figure 1. It has been found that fullerene derivatives are able to suppress disease onset and to reverse established disease in murine asthma models by decreasing airway inflammation and bronchoconstriction. Therefore, we speculate that fullerene molecules can interact with β_2 AR for the treatment of asthma with associated inflammation. Moreover, Yamawaki et al [41] found that the derivative C₆₀(OH)₂₄ caused cytotoxic injury or cell death in vascular endothelial cells, indicating that exposure to fullerene could represent a risk for atherosclerosis and ischemic heart disease. Furthermore, Wang et al [42] found that the ECL2 (extracellular loop 2) and the transmembrane helix 7 (TM7) in β_2 AR formed a hydrophobic bridge upon the entry site of the ligand. Moreover, the extracellular top of the binding pocket was shown to be composed of rich hydrophobic residues such as PHE, TYR and LYS. Inspired by the structural features of β_2 AR, we postulate that C₆₀ molecules could interact with β_2 AR through hydrophobic interaction. The ligands of β_2 AR are mainly bound by polar hydrogen bonds, so the polar fullerene derivatives may also interact with the β_2 AR. Therefore, it is necessary to study the interaction between β_2 AR and fullerene or its hydroxyl derivatives.

Due to the complexity of the biosystem, it is not practical to investigate experimentally the effects of fullerenes and fullerene derivatives upon β_2 AR. Computer simulation can be a good alternative. Although there have been large quantities of results describing the interactions between C₆₀ and proteins observed by experimental and computational methods, no research has been reported focusing on the interaction between C₆₀ and β_2 AR. In this work, we used MD simulation to investigate the interactions of fullerene and its

hydroxyl derivatives with β_2 AR, to elucidate their toxic effect on the function of β_2 AR based on the simulated trajectories. We mainly aimed to address the following issues: (1) identification of the binding sites of C_{60} , $C_{60}(\text{OH})_4$, and $C_{60}(\text{OH})_8$ in β_2 AR; (2) the effects of mono- C_{60} , five $C_{60}\text{S}$, $C_{60}(\text{OH})_4$, and $C_{60}(\text{OH})_8$ on the structure of β_2 AR; (3) whether or not C_{60} and $C_{60}(\text{OH})_X$ ($X = 4, 8$) compete with the binding site of β_2 AR; (4) whether C_{60} and $C_{60}(\text{OH})_X$ ($X = 4, 8$) block protein entry.

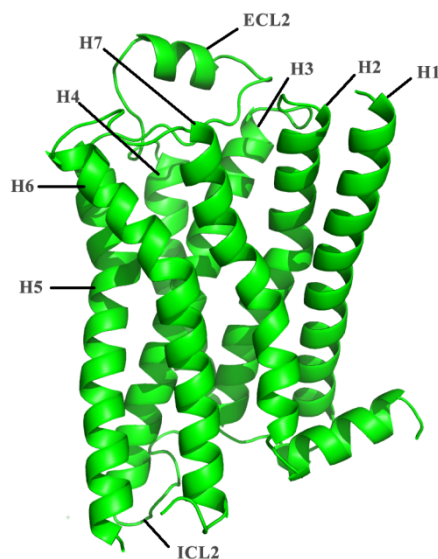


Figure 1. The crystal structure of β_2 AR (PDB ID: 2RH1) and the seven transmembrane helices H1–H7, as well as the ECL2 and ICL2 loops.

2. Simulation Details

2.1. Construction of Fullerene and Derivative Models

The initial structures of C_{60} fullerene (with radius 3.48 Å) and its hydroxyl derivatives $C_{60}(\text{OH})_X$ ($X = 4$ or 8) were built as shown in Figure 2, where X means the number of hydroxyl groups. For the derivative $C_{60}(\text{OH})_4$ with four hydroxyls, we constructed two representative models $C_{60}(\text{OH})_{4_1}$ and $C_{60}(\text{OH})_{4_2}$, with their hydroxyl groups located at different surface positions of C_{60} . In the model $C_{60}(\text{OH})_{4_1}$, the four hydroxyls were located at the close positions of the fullerene spherical surface, with two or three carbon atoms between the two adjacent hydroxyls. In the other model $C_{60}(\text{OH})_{4_2}$, the four hydroxyls were evenly distributed spherical fullerenes. For the $C_{60}(\text{OH})_8$ model, there were four hydroxyls close to each other, but the other four hydroxyls were far from each of these four hydroxyls. The structures of fullerene and derivatives were optimized using the B3LYP/6-31G* method in the Gaussian09 software [43]. Then, frequency analysis was carried out to obtain the vibrational force constants for all the bonds and angles involved in the fullerene and derivatives. The RESP charges of all atoms in the fullerenes and derivatives were calculated by fitting the molecular electrostatic potential [44,45]. The van der Waals interactions of pairwise atoms were described using the classical Lennard-Jones potential. The parameters of the cross section s and well depth ϵ in the Lennard-Jones potential were taken from the Amber03 force field, with values of 0.34 nm and 0.36 kJ/mol respectively.

2.2. Simulation Systems

The initial structure of β_2 AR was extracted from the crystal structure (PDB ID: 2RH1) deposited in the online Protein Data Bank [46]. The crystal structure of β_2 AR contains an endogenous ligand (–)-Isoproterenol [47,48], which is a beta adrenoreceptor agonist used for the treatment of bradycardia (slow heart rate), heart block, and asthma. The (–)-Isoproterenol in the system is abbreviated as ‘IPT’.

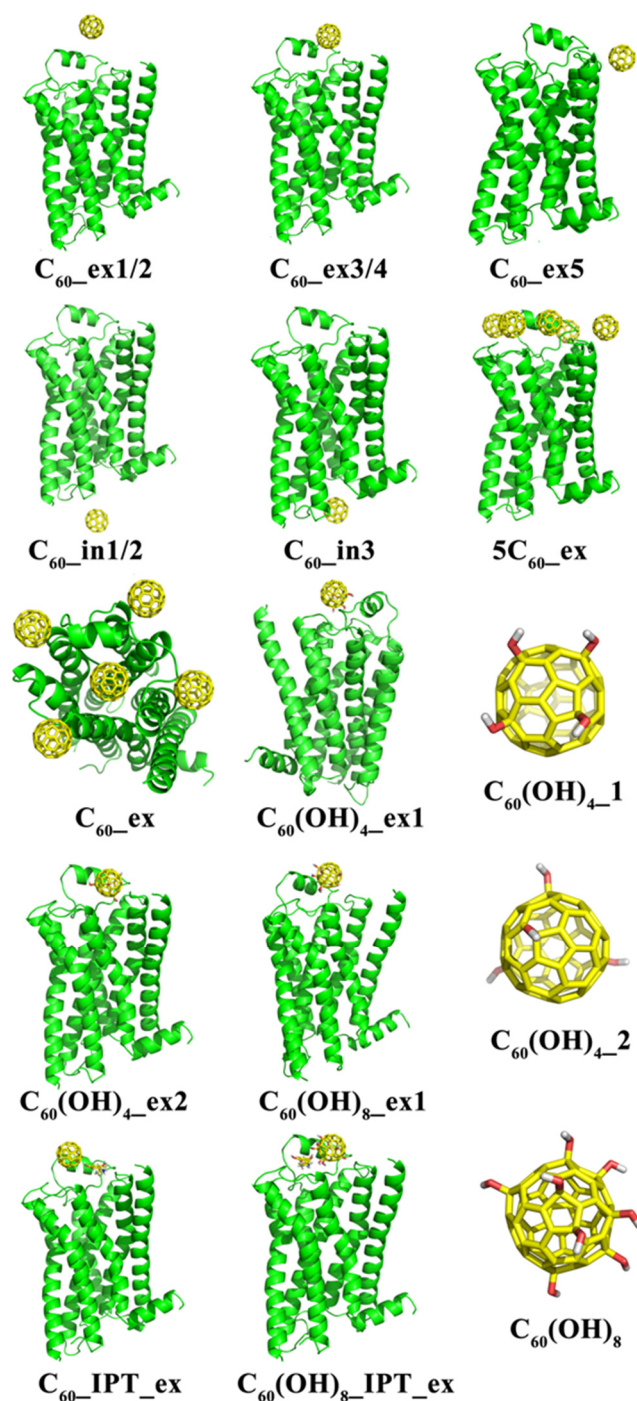


Figure 2. The initial structures of the fullerene derivatives $C_{60}(OH)_4-1$, $C_{60}(OH)_4-2$ and $C_{60}(OH)_8$ for simulation.

To explore systematically the interaction of the β_2AR protein with the fullerene and derivatives, we constructed fifteen systems composed of β_2AR protein complexes, DOPC lipids and water molecules. Details of the components in these complex systems are shown in Table 1.

In these complex systems, the initial positions of fullerenes and derivatives were randomly placed at the extracellular or intracellular sides of lipid membranes, indicated by “ex” or “in” in the notation. Initially, to reduce the interaction between the fullerene molecule or fullerene derivatives and β_2AR , they were spatially separated at distances (defined as the distance between the center of fullerene or derivative’s mass and the β_2 -

adrenergic receptor surface) of 1.4 nm for C₆₀_ex1 (C₆₀_ex2), 0.7 nm for C₆₀_ex3 (C₆₀_ex4), 0.9 nm in C₆₀_in1 (C₆₀_in2), 1.0 nm for C₆₀_IPT_ex, and 0.8 nm for C₆₀(OH)₈_IPT_ex. In the simulation of C₆₀_ex5, the fullerene was in the middle of the ECL1 of β_2 AR and the neighboring lipid membranes. The centroid distance between the fullerene and the lipid membrane corresponded to the membrane thickness at the position of the lipid membrane surface. The fullerene of C₆₀_in3 was put on the top of the pocket using the helix3, helix4, helix6, and helix7. The IPT of the system C₆₀_IPT_ex, C₆₀(OH)₈_IPT_ex was manually placed at the top of the binding pocket. The specific positions of C₆₀, C₆₀(OH)₄, and C₆₀(OH)₈ IPT molecules in the corresponding systems are shown in Figure 2.

Table 1. Details of the constructed complex systems composed of fullerene, fullerene derivatives and β_2 AR, with the 122 DOPC lipids and different numbers of water molecules.

Notations	Components	Number of DOPCs/Waters
Pure_ β_2 AR	Without fullerene or fullerene derivative	122/12274
C ₆₀ _ex1, C ₆₀ _ex2	One C ₆₀ in the extracellular side	122/12274
C ₆₀ _ex3, C ₆₀ _ex4	One C ₆₀ in the extracellular side	122/12202
C ₆₀ _ex5	One C ₆₀ in the extracellular side	122/12113
C ₆₀ _in1, C ₆₀ _in2	One C ₆₀ in the intracellular side	122/12035
C ₆₀ _in3	One C ₆₀ in the intracellular side	122/11542
C ₆₀ (OH) ₄ _ex1	One C ₆₀ with 4 OH in the extracellular side	122/11153
C ₆₀ (OH) ₄ _ex2	One C ₆₀ with 4 OH in the extracellular side	122/11375
5C ₆₀ _ex	Five C ₆₀ s in the extracellular side	122/13899
C ₆₀ (OH) ₈ _ex1	One C ₆₀ with 8 OH in the extracellular side	122/12059
C ₆₀ _IPT_ex	One C ₆₀ and one isoproterenol in the extracellular side	122/12308
C ₆₀ (OH) ₈ _IPT_ex	One C ₆₀ with 8 OH and one isoproterenol molecule in the extracellular side	122/12902

2.3. Simulation Details

The MD simulations for all systems were carried out using the Amber03 force field in the Gromacs 4.4.5 software [49]. In the simulation, the bonds involving hydrogen atoms were constrained using the LINCS protocol [50] and the non-bonded interactions were updated every five integration steps. The DOPC bilayers, fullerenes, β_2 ARs, and water molecules were coupled to the Berendsen thermostat [51] at 300 K with a relaxation time of 0.1 ps. The surface tension of bilayer liquids was maintained at a magnitude of 440 bar/nm. The pressure perpendicular to the liquid surface was kept at 1.0 bar using Berendsen pressure coupling with a relaxation time of 1.0 ps and a water compressibility of $4.5 \times 10^{-5} \text{ bar}^{-1}$. The electrostatic interaction of pairwise atoms was estimated using the Particle Mesh Ewald method, and van der Waals interaction within a cutoff 1.2 nm was taken into account. All the systems were first energy-minimized, then heated to 300 K and equilibrated for 300 ns in the NPT ensembles. All data in figures were analyzed based on the equilibrated trajectories of 300 ns MD simulations.

3. Result and Discussion

3.1. Binding Sites of Monomeric Fullerenes upon β_2 AR

Figure 3 shows the various binding patterns of monomeric fullerenes to the β_2 AR proteins. The C₆₀ molecules in these plots display the final positions in snapshots extracted from MD trajectories. It can be clearly seen that the binding sites of fullerenes were mainly located near the ECL2 or ICL2, except for the system C₆₀_in1. During the MD simulations, the positions of fullerenes in C₆₀_ex1/2/3/4/5 and C₆₀_in2/3 showed almost no large changes compared to their initial positions. The reason for this might be the fact that the β_2 AR is a polar receptor, so it prevents the nonpolar C₆₀ from entering. As shown in the MD simulations, the C₆₀ molecules in the aqueous phase attached quickly to β_2 ARs within 5 ns. Since the binding pockets of β_2 AR are hydrophilic, the C₆₀ molecules prefer to bind to the exposed ECL2 instead of entering it. Figure 4 shows the structural details of the

specific amino acids at the binding sites of β_2 AR in $C_{60_ex1/2}$, $C_{60_ex3/4}$, C_{60_ex5} and C_{60_in2} interacting with C_{60} . It can be seen that the C_{60} molecules were embedded in the cavities formed by the hydrophobic moieties of polar and non-polar amino acids such as GLN, MET, and PHE of ECL2. The aromatic rings of the TYR residues in $C_{60_ex3/4}$, PHE in C_{60_ex5} , and PHE of ICL2 in C_{60_in2} formed the π - π stacking interaction to stabilize the conformations of C_{60} .

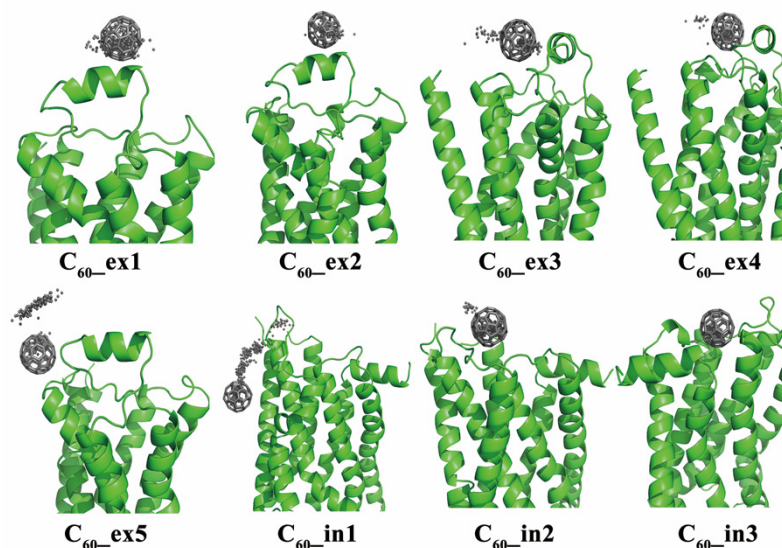


Figure 3. The initial binding sites of monomeric fullerenes in different systems of protein complexes. The black dots represent the center of mass of C_{60} along the MD trajectory sampled every 1 ns and the stick is the ending position of C_{60} .

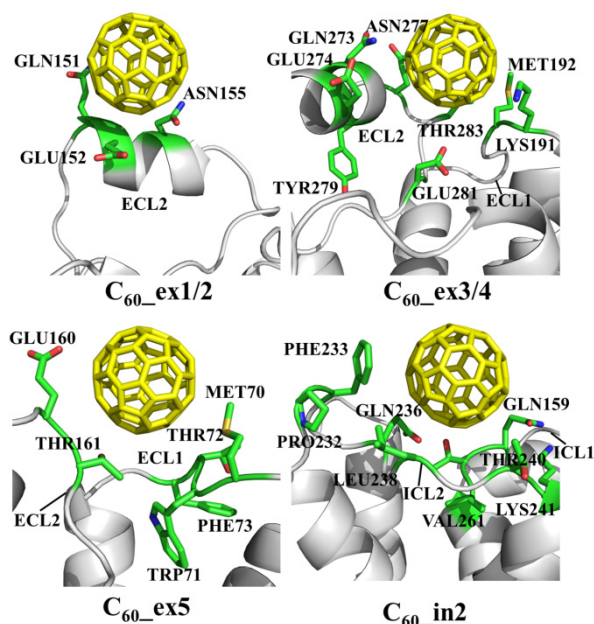


Figure 4. Snapshots of the $C_{60_ex1/2}$, $C_{60_ex3/4}$, C_{60_ex5} and C_{60_in2} systems show that the key amino acids of the ECL1 and ECL2 interact with the monomeric fullerenes at the extracellular and intracellular sides.

In Figure 3, it can be observed that the C_{60} in the C_{60_in1} simulation eventually entered the lipid membrane, which differed from the C_{60_in2} simulation with the same initial structure. To gain insight into the dynamic process of C_{60} entry into the membrane,

we extracted a series of snapshots from the MD trajectory and marked the positions of C_{60} at different simulation times using different colors, as shown in Figure 5. The illustration shows that C_{60} gradually squeezed into the lipid membrane during the 300 ns simulation.

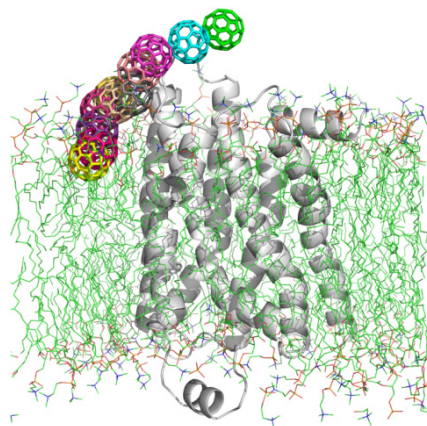


Figure 5. The traced positions of C_{60} extracted from the snapshots of simulated trajectory of the C_{60} -in1 system. The green and yellow models represent the initial and final positions, respectively.

Figure 6 shows the positions of fullerenes in the snapshots extracted from the MD trajectory, with the specific residues surrounded. In the snapshots at 1 ns and 30 ns, the C_{60} molecules showed strong packing interaction with the aromatic rings of PRO and PHE residues. Subsequently, the C_{60} molecules gradually moved away from the ICL2 region, and embedded deeply to interact with the hydrophobic residues in helix4, such the PHE and VAL residues. It can be seen that the loop in the ICL2 region completely flipped after 50 ns, so that the interaction became weak. Finally, the C_{60} molecule was bound to the hydrophobic PHE, TYR, and VAL residues in the helix4, and its conformation changed remarkably.

3.2. Binding Sites of Multiple Fullerenes upon β_2 AR

Using a high concentration of fullerenes in experiments, multiple C_{60} molecules should be present to interact with the β_2 AR protein. To explore the interaction mechanism, we randomly placed five C_{60} molecules at the extracellular side of β_2 AR at the beginning of the MD simulation. The separation between C_{60} molecules was beyond 15 Å, and the distances between the centroids of C_{60} and the protein surface was about 7 Å. Figure 7 shows the traces of C_{60} molecules as well as the final stable conformations. The traced dots indicate that although the initial structures of C_{60} were separated far apart from each other, four of them, i.e., C_{60_2} , C_{60_3} , C_{60_4} and C_{60_5} , finally tended to form a C_{60} cluster. In particular, the cyan dots reveal that the C_{60_2} moved nearly 25 Å from its initial position and finally formed a stable cluster with other C_{60} molecules. C_{60_1} could not move around and was trapped in a local stable conformation due to the obstacle of ECL2.

The simulation result shown in Figure 7 indicates that the multiple C_{60} molecules tended to form aggregates at the surface of β_2 AR because of their strong hydrophobic effect. Thus, the hydrophobic surface of C_{60} preferred to interact with the hydrophobic surface of β_2 AR, so that the entropy of the whole protein–protein interaction was most favorable. Furthermore, the simulation revealed that the formed C_{60} cluster remained at the entrance of the β_2 AR binding site, meaning that the high concentration of C_{60} molecules might block the ligand binding to β_2 AR and interrupt the function of β_2 AR.

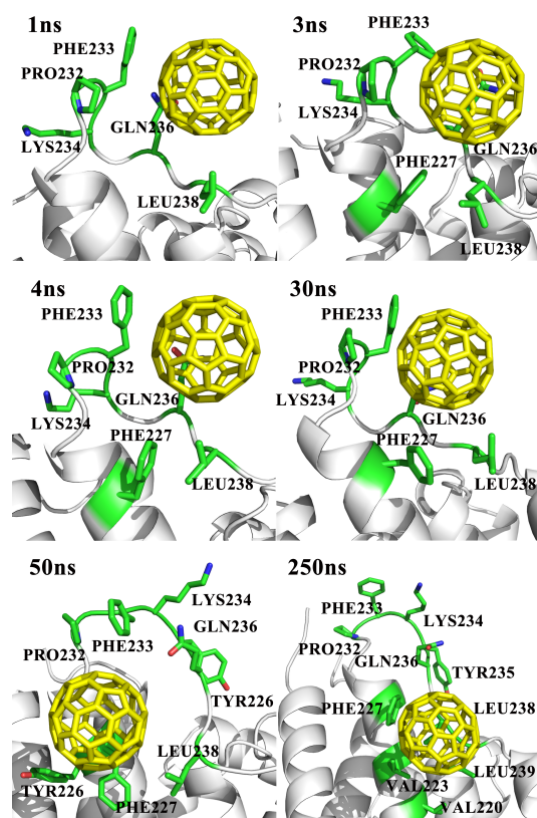


Figure 6. Snapshots of the system C₆₀_in1 at different simulation times show that the key amino acids such as the PRO232, PHE233, LYS234, GLN236 and LEU238 interacted with the monomeric fullerenes at the extracellular and intracellular sides.

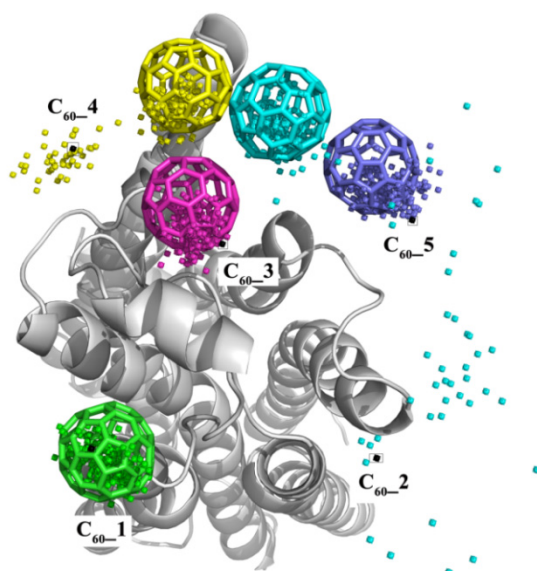


Figure 7. The trajectory of five fullerene molecules in the 5C₆₀_ex system (top view); different colors represent different fullerene molecules. Each dot represents the average position (center of mass) of C₆₀ along the MD trajectory, sampled every 1 ns. The black dots represent the initial positions and the colored stick is the final position of C₆₀.

3.3. Binding Sites of Fullerene Derivatives upon β_2 AR

Because C₆₀ is nonpolar, the major interaction of fullerene with β_2 AR is hydrophobic. This does not hold true for the fullerene derivatives, since the derivatives C₆₀(OH)_X (X = 4

or 8) possess polar hydroxyl groups on their surfaces. Figure 8 shows the stable interaction patterns of $C_{60}(OH)_4_ex1$, $C_{60}(OH)_4_ex2$, and $C_{60}(OH)_8$ with the β_2AR proteins. It appears that the binding capacity of fullerene derivatives was stronger than that of C_{60} molecules. For example, the hydroxyl groups in $C_{60}(OH)_4_ex1$ formed hydrogen bonds with the GLU and ASN residues in ECL2. In $C_{60}(OH)_4_ex2$, the hydroxyl groups formed hydrogen bonds with the ASP, GLU, and THR residues, and in $C_{60}(OH)_8_ex$, the hydroxyl groups interacted with the HIE, LYS, ASP, and CYX residues. The hydroxyl groups in the fullerene derivatives acted like claws and firmly hooked β_2AR so that the derivatives blocked the entrance of the β_2AR binding channels.

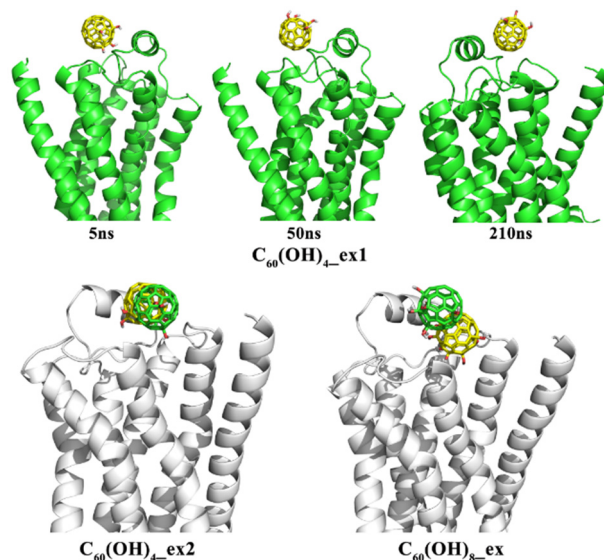


Figure 8. Three snapshots of $C_{60}(OH)_4_ex1$ at different simulation times are shown above, and the two systems $C_{60}(OH)_4_ex2$ and $C_{60}(OH)_8$ are shown below. The green and yellow models of $C_{60}(OH)_X$ ($X = 4, 8$) represent initial and final positions, respectively.

Although $C_{60}(OH)_4_ex1$ and $C_{60}(OH)_4_ex2$ each contain four hydroxyl groups, their interaction patterns with β_2AR were not entirely similar. In the first 40 ns, the four hydroxyl groups in $C_{60}(OH)_4_ex1$ formed hydrogen bonds with β_2AR . After 50 ns, the hydrogen bonds between $C_{60}(OH)_4_ex1$ and β_2AR were broken and the hydroxyl groups pointed toward the aqueous phase. This phenomenon was not observed in the simulation of $C_{60}(OH)_4_ex2$, in which the four hydroxyl groups were located far away from each other. By analyzing the interaction between $C_{60}(OH)_4_ex2$ and β_2AR , we found that the strong hydrogen bonds formed between $C_{60}(OH)_4_ex2$ and the ASP164 and GLU152 residues in ECL2 were retained throughout the 300 ns simulation, which maintained the stable conformation of $C_{60}(OH)_4_ex2$. Comparison of the MD simulations of $C_{60}(OH)_4_ex1$ and $C_{60}(OH)_4_ex2$ revealed that the position of hydroxyl groups had a great influence on the binding capacity of fullerene derivatives. When the hydroxyl groups on the surface of C_{60} stayed close to each other, stable hydrogen bond interaction with β_2AR was difficult to maintain, due to the steric effect.

Meanwhile, the number of hydroxyl groups might affect the binding capacity of derivatives to β_2AR . In order to explore the dependence of binding capacity on the number of hydroxyl groups, we also carried out MD simulation for the $C_{60}(OH)_8_ex$ system, as shown in Figure 8. This showed that the $C_{60}(OH)_8$ molecule was deeply embedded in the β_2AR . The hydroxyl groups behaved like several claws firmly grasping the β_2AR , blocking the binding entry of ligands. Strong hydrogen bonds formed between the hydroxyl groups and each of the residues ASP164 and GLU152, and were not broken during the 300 ns simulation time. The difference between $C_{60}(OH)_4_ex2$ and $C_{60}(OH)_8_ex$ indicates that

increasing the number of hydroxyl groups in fullerenes could enhance their ability to bind with β_2 AR.

3.4. Stability of β_2 AR with Binding

To explore the effect of fullerene binding, and that of its derivatives, on the stability of β_2 AR, we calculated the RMSDs of β_2 AR backbones for the eight systems, as shown in Figure 9. The RMSDs of all curves, except the C_{60_in1} system, remained around 0.2 nm in the simulations, consistent with the results simulated by Romo et al [52]. The RMSD values fluctuated around 0.2 nm, indicating that the cores of β_2 AR were extremely rigid and less susceptible to external binding with C_{60} and its derivatives. For the system C_{60_in1} , the RMSD reached 0.27 nm at 300 ns, a little higher than that of pure β_2 AR. The large RMSD change exhibited by β_2 AR in C_{60_in1} was caused by the hydrophobic interaction of the ICL2 and helix3 with C_{60} . In contrast, the RMSD values of C_{60_in3} were relatively lower than those of the pure β_2 AR system. The reason for this lies in the fact that the fullerene molecule in C_{60_in3} was trapped in the cavity formed by helix 3, helix 4, helix 6 and helix 7, which hindered the cooperative movement of helices in β_2 AR. Previous studies reported that β_2 AR could be activated by the cooperative movement of seven helices, and the ligand binding relied on the collaborative movement of seven helices [53–56].

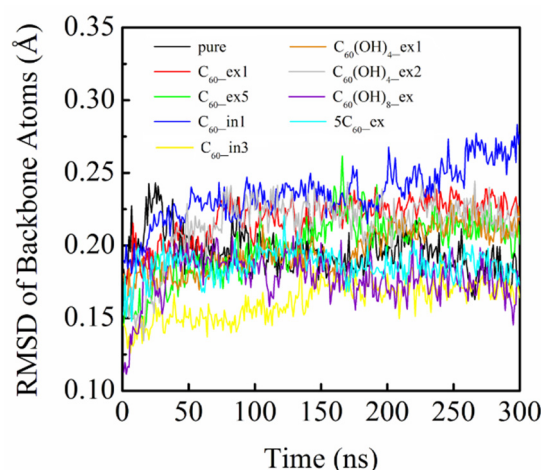


Figure 9. The calculated RMSD curves of the entire protein backbones with respect to the β_2 AR crystal structure.

We further analyzed the RMSD change of secondary structures of β_2 AR, especially for the key helix4. Figure 10 clearly shows the average structural changes of helix4 in each system, with respect to the crystal structure as a reference. It can be observed that the helix4 in the pure β_2 AR showed no remarkable structural change, while those in C_{60_ex2} , C_{60_ex3} , C_{60_ex4} , C_{60_in2} , C_{60_in3} , $C_{60(OH)_8_ex}$, and $5C_{60_ex}$ changed little. However, the helices in C_{60_ex1} , C_{60_ex5} , C_{60_in1} , $C_{60(OH)_4_ex1}$, and $C_{60(OH)_4_ex2}$ were severely distorted from the crystal structures. Figure 11 shows the RMSD values of helices 4 calculated for the nine systems in Figure 9. The RMSD change of helix4 for $C_{60(OH)_4_ex1/2}$ was larger than that of $C_{60(OH)_8_ex}$. This could be attributed to the strong hydrogen bonding interaction between $C_{60(OH)_8}$ and β_2 AR in $C_{60(OH)_8_ex}$. In addition, the C_{60} cluster formed in $5C_{60_ex}$ had no substantial influence on the stability of helix 4. This suggests that increasing the number of C_{60} molecules has minimal influence on the stability of β_2 AR.

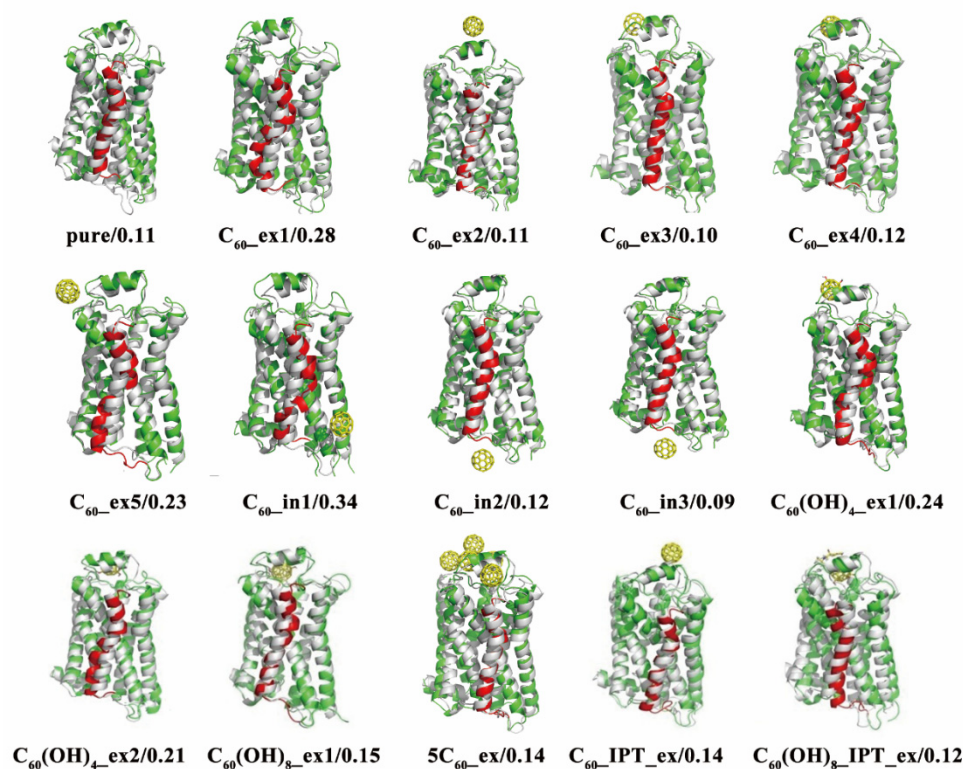


Figure 10. The conformational changes of the simulated systems. The gray parts of the illustrations denote the crystal structures, and the last snapshots in the simulated system trajectories are shown in green, with the helix4 of each highlighted in red. The yellow models represent C₆₀ and C₆₀(OH)_X molecules, and the RMSD values of helix4 with respect to the crystal structure are listed below the structures.

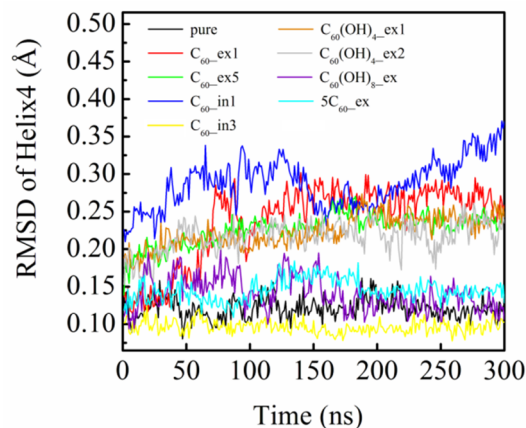


Figure 11. The calculated RMSD curves of helix4 in nine systems with respect to the β_2 AR crystal structure.

To uncover the mechanism of the helix4 structural change, we analyzed the conformation evolution of β_2 AR, as shown in Figure 12. We found that it was closely associated with the conformational change of the key residue PHE193 in ECL2. The PHE193 showed an obvious flip in C₆₀-ex1, C₆₀-in1, and C₆₀(OH)₄-ex1. Compared to the RMSD curves in Figure 11, we found that these three systems had large RMSD values for the fluctuation of helix4. This is because the fullerene molecules outside the membrane underwent hydrophobic and π - π stacking interaction with PHE193, and the fullerene molecules in the membrane mainly affected the structure of helix4 by changing the structure of ICL2.

Therefore, it was postulated that the structural changes of helix4 would be directly related to the structural changes of PHE193.

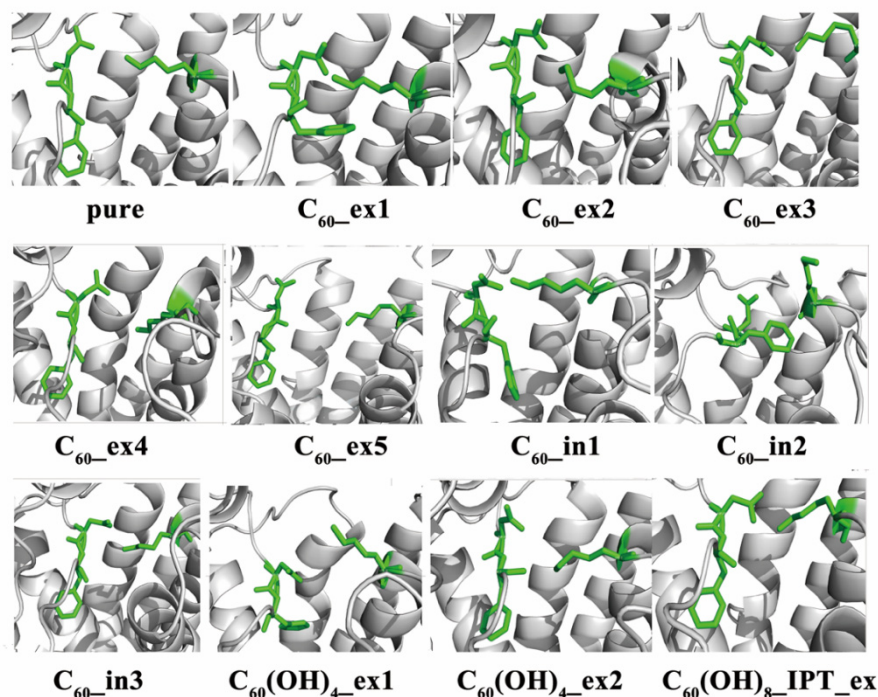


Figure 12. The conformations of PHE193 in snapshots at the final 1 ns.

3.5. Competitive Mechanism of $C_{60}/C_{60}(OH)_8$ and Isoproterenol

Previous experiments have shown that fullerene molecules and fullerene derivatives may compete with ligands for protein binding sites. In our study, we built two systems, labeled as $C_{60_IPT_ex}$ and $C_{60}(OH)_8_IPT_ex$, to investigate the competitive mechanisms of C_{60} and $C_{60}(OH)_8$. Here 'IPT' is used as the abbreviated name for isoproterenol. Although, the C_{60} molecule and isoproterenol were both placed above the binding site, we found that C_{60} acted as a single fullerene and had no influence on the isoproterenol within the simulation time, as shown in Figure 13. This result can easily be understood by the hydrophobic nature of pure C_{60} . Then we placed $C_{60}(OH)_8$ and isoproterenol together, and found that $C_{60}(OH)_8$ quickly combined with β_2AR through hydrogen bonds, and the isoproterenol was relegated to the outside. It is interesting that the benzene ring and $C_{60}(OH)_8$ were packed together. When there were many hydroxyl fullerene derivatives outside the cell membrane, they were likely to compete with ligands for the binding site, thus affecting the signal transduction of β_2AR to the following proteins.

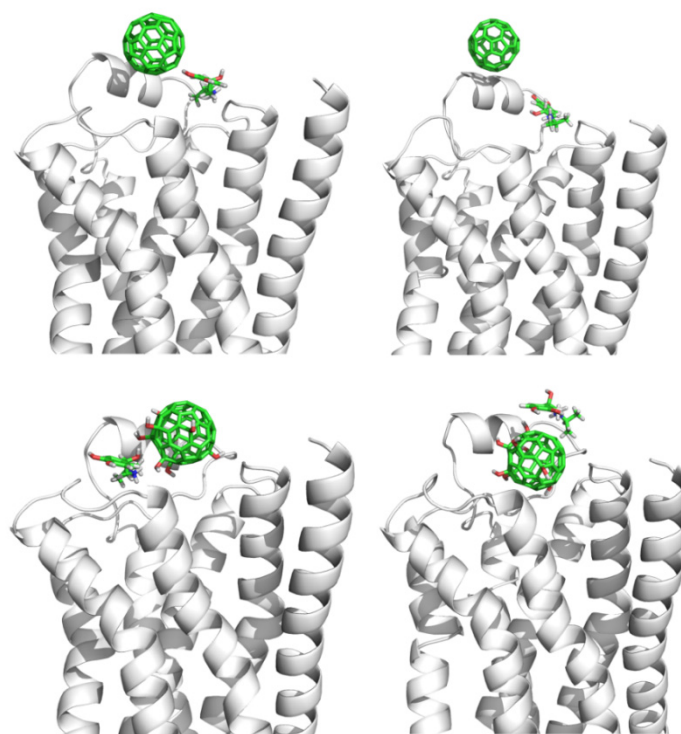


Figure 13. The initial (**left**) and final (**right**) structures of the C_{60} _IPT_ex (**upper**) and $C_{60}(\text{OH})_8$ _IPT_ex (**lower**) systems. The C_{60} , $C_{60}(\text{OH})_8$, and isoproterenols are colored green and the β_2 ARs are grey.

4. Conclusions

In this work, we studied for the first time the interactions between fullerene and fullerene derivatives and β_2 AR, using a series of all-atom MD simulations. We established fifteen systems by placing fullerene and fullerene derivatives at different positions outside and inside the membrane. Our results show that the unmodified fullerene was unable to enter the ligand binding sites, instead mainly binding with the loop of ECL2 and ICL2 on β_2 AR through hydrophobic interactions and π - π stacking interactions, especially with residue PHE193 on ECL2, and PHE and PRO residues on ICL2. In addition to having a strong hydrophobic interaction with nonpolar amino acid residues, fullerene molecules also underwent obvious hydrophobic interaction with hydrophobic carbon atoms on polar amino acids, such as GLN, GLU, ASP, LYS, TYR, and THR. In most cases (except C_{60} _in1), fullerene and derivatives did not enter the lipid membrane, but remained around the β_2 AR. In the C_{60} _in1 trajectory, due to the π - π stacking interactions of the fullerene molecule with PHE and PRO residues on ICL2, ICL2 completely flipped towards the fullerene direction along with the movement of fullerene slowly into the lipid membrane. Five fullerenes tended to stack into a stable fullerene cluster (a deformed tetrahedral aggregate) rather than interacting alone with β_2 AR. In addition, as the simulation time extended, the position of the fullerene aggregates became almost motionless, just above the receptor binding pocket, which would block the movement of ligands into protein channels and hinder the ligands' binding to proteins. The binding capacity between polyhydroxy derivatives and β_2 AR was stronger compared with unmodified fullerene molecules.

The hydroxyl groups of fullerene derivatives $C_{60}(\text{OH})_4$ and $C_{60}(\text{OH})_8$ can form strong hydrogen bonds with the ECL2, helix6, and helix 7 of 2AR. The hydroxyl groups firmly grasped the β_2 AR receptor like several claws, blocking the binding entry of ligands. The position and number of hydroxyl groups on fullerene derivatives also seriously affected the interaction between the two groups. The more dispersed the hydroxyl position and the greater the hydroxyl number, the stronger was the binding activity with the β_2 AR.

We further explored the effect of fullerene and its derivatives on β_2 AR structure. The results indicated that fullerenes and their derivatives did not have an obvious impact

on the whole structure of the receptor, but could affect the structure of helix4 in some systems, especially in the systems C₆₀_ex1, C₆₀_ex5, C₆₀_in1, C₆₀_in3, C₆₀(OH)₄_ex1, and C₆₀(OH)₄_ex2. The helix4 structures in the above systems were seriously distorted, with the upper part twisted to the right, and the lower part distorted to the left. Moreover, the more hydroxyl in the fullerene derivative, the smaller was the effect on the β_2 AR structure.

In summary, fullerenes and fullerene derivatives can interact with β_2 AR by hydrophobic interactions, π - π stacking interactions and hydrogen bonding. This combination may block the entry of ligands into protein binding sites, and also may compete with ligands for binding sites, thereby affecting the normal biological function of β_2 AR. Therefore, in future medical research it is important to consider the effect of fullerene and its derivatives on β_2 AR, to further reduce its toxicity to biological cells.

Author Contributions: Conceptualization, Z.J.; investigation, Y.L.; writing, L.R.; project administration, F.X.; supervision, J.Z.Z.; funding acquisition, Y.L. All authors have read and agreed to the published version of the manuscript.

Funding: This work was supported by the Natural Science Foundation of Shandong Province (ZR2020MA075, ZR2020QA051), National Natural Science Foundation of China (12104262). We acknowledge the support of the NYU-ECNU center for Computational Chemistry at NYU Shanghai. We also thank the supercomputer center of ECNU for providing computer time.

Institutional Review Board Statement: Not applicable.

Informed Consent Statement: Not applicable.

Data Availability Statement: The data presented in this study are available on request from the corresponding author. The data are not publicly available due to privacy.

Conflicts of Interest: The authors declare no conflict of interest.

Sample Availability: Not applicable.

References

1. Kroto, H. Space, Stars, C₆₀, and Soot. *Science* **1988**, *242*, 1139–1145. [[CrossRef](#)] [[PubMed](#)]
2. Kroto, H.W.; Heath, J.R.; O'Brien, S.C.; Curl, R.F.; Smalley, R.E. C₆₀: Buckminsterfullerene. *Nature* **1985**, *318*, 162–163. [[CrossRef](#)]
3. Ye, L.J.; Kollie, L.; Liu, X.; Guo, W.; Ying, X.X.; Zhu, J.; Yang, S.J.; Yu, M.L. Antitumor Activity and Potential Mechanism of Novel Fullerene Derivative Nanoparticles. *Molecules* **2021**, *26*, 3252. [[CrossRef](#)] [[PubMed](#)]
4. Nozdrenko, D.; Abramchuk, O.; Prylutska, S.; Vygovska, O.; Soroca, V.; Bogutska, K.; Khrapatyi, S.; Prylutsky, Y.; Scharff, P.; Ritter, U. Analysis of Biomechanical Parameters of Muscle Soleus Contraction and Blood Biochemical Parameters in Rat with Chronic Glyphosate Intoxication and Therapeutic Use of C₆₀ Fullerene. *Int. J. Mol. Sci.* **2021**, *22*, 4977. [[CrossRef](#)]
5. Bakry, R.; Vallant, R.M.; Najam-ul-Haq, M.; Rainer, M.; Szabo, Z.; Huck, C.W.; Bonn, G.K. Medicinal applications of fullerenes. *Int. J. Nanomed.* **2007**, *2*, 639–649.
6. Anilkumar, P.; Lu, F.; Cao, L.; Luo, P.G.; Liu, J.H.; Sahu, S.; Tackett, K.N., II; Wang, Y.; Sun, Y.P. Fullerenes for Applications in Biology and Medicine. *Curr. Med. Chem.* **2011**, *18*, 2045–2059. [[CrossRef](#)]
7. Kumar, M.; Raza, K. C₆₀-fullerenes as Drug Delivery Carriers for Anticancer Agents: Promises and Hurdles. *Pharm. Nanotechnol.* **2017**, *5*, 169–179. [[CrossRef](#)]
8. Alipour, E.; Alimohammady, F.; Yumashev, A.; Maseleno, A. Fullerene C₆₀ containing porphyrin-like metal center as drug delivery system for ibuprofen drug. *J. Mol. Model.* **2020**, *26*, 7. [[CrossRef](#)]
9. Friedman, S.H.; Decamp, D.L.; Sijbesma, R.P.; Srdanov, G.; Wudl, F.; Kenyon, G.L. Inhibition of the HIV-1 Protease by Fullerene Derivatives—Model-Building Studies and Experimental-Verification. *J. Am. Chem. Soc.* **1993**, *115*, 6506–6509. [[CrossRef](#)]
10. Ibrahim, M.; Saleh, N.A.; Elshemey, W.M.; Elsayed, A.A. Fullerene Derivative as Anti-HIV Protease Inhibitor: Molecular Modeling and QSAR Approaches. *Mini-Rev. Med. Chem.* **2012**, *12*, 447–451. [[CrossRef](#)]
11. Yasuno, T.; Ohe, T.; Kataoka, H.; Hashimoto, K.; Ishikawa, Y.; Furukawa, K.; Tateishi, Y.; Kobayashi, T.; Takahashi, K.; Nakamura, S.; et al. Fullerene derivatives as dual inhibitors of HIV-1 reverse transcriptase and protease. *Bioorg. Med. Chem. Lett.* **2021**, *31*, 127675. [[CrossRef](#)] [[PubMed](#)]
12. Ryan, J.J.; Bateman, H.R.; Stover, A.; Gomez, G.; Norton, S.K.; Zhao, W.; Schwartz, L.B.; Lenk, R.; Kepley, C.L. Fullerene nanomaterials inhibit the allergic response. *J. Immunol.* **2007**, *179*, 665–672. [[CrossRef](#)] [[PubMed](#)]
13. Norton, S.K.; Wijesinghe, D.S.; Dellinger, A.; Sturgill, J.; Zhou, Z.; Barbour, S.; Chalfant, C.; Conrad, D.H.; Kepley, C.L. Epoxyeicosatrienoic acids are involved in the C₇₀ fullerene derivative-induced control of allergic asthma. *J. Allergy Clin. Immunol.* **2012**, *130*, 761–769.e2. [[CrossRef](#)] [[PubMed](#)]

14. Dellinger, A.L.; Cunin, P.; Lee, D.; Kung, A.L.; Brooks, D.B.; Zhou, Z.; Nigrovic, P.A.; Kepley, C.L. Inhibition of Inflammatory Arthritis Using Fullerene Nanomaterials. *PLoS ONE* **2015**, *10*, e0126290. [[CrossRef](#)] [[PubMed](#)]
15. Wang, Q.L.; Zhang, P.; Ansari, M.J.; Aldawsari, M.F.; Alalaiwe, A.S.; Kaur, J.; Kumar, R.; Lup, A.N.K.; Enayati, A.; Mirzaei, H.; et al. Electrostatic interaction assisted Ca-decorated C₂₀ fullerene loaded to anti-inflammatory drugs to manage cardiovascular disease risk in rheumatoid arthritis patients. *J. Mol. Liq.* **2022**, *350*, 118564. [[CrossRef](#)]
16. Dellinger, A.; Zhou, Z.; Connor, J.; Madhankumar, A.B.; Pamujula, S.; Sayes, C.M.; Kepley, C.L. Application of fullerenes in nanomedicine: An update. *Nanomedicine* **2013**, *8*, 1191–1208. [[CrossRef](#)]
17. Johnston, H.J.; Hutchison, G.R.; Christensen, F.M.; Aschberger, K.; Stone, V. The Biological Mechanisms and Physicochemical Characteristics Responsible for Driving Fullerene Toxicity. *Toxicol. Sci.* **2010**, *114*, 162–182. [[CrossRef](#)]
18. Prylutska, S.V.; Grebinyk, A.G.; Lynchak, O.V.; Byelinska, I.V.; Cherepanov, V.V.; Tauscher, E.; Matyshevska, O.P.; Prylutsky, Y.I.; Rybalchenko, V.K.; Ritter, U.; et al. In vitro and in vivo toxicity of pristine C₆₀ fullerene aqueous colloid solution. *Fuller. Nanotub. Carbon Nanostruct.* **2019**, *27*, 715–728. [[CrossRef](#)]
19. Oberdorster, E. Manufactured nanomaterials (Fullerenes, C₆₀) induce oxidative stress in the brain of juvenile largemouth bass. *Environ. Health Perspect.* **2004**, *112*, 1058–1062. [[CrossRef](#)]
20. Sumi, N.; Chitra, K.C. Possible role of C₆₀ fullerene in the induction of reproductive toxicity in the freshwater fish, *Anabas testudineus* (Bloch, 1792). *Environ. Sci. Pollut. Res.* **2020**, *27*, 19603–19615. [[CrossRef](#)]
21. Fortner, J.D.; Lyon, D.Y.; Sayes, C.M.; Boyd, A.M.; Falkner, J.C.; Hotze, E.M.; Alemany, L.B.; Tao, Y.J.; Guo, W.; Ausman, K.D.; et al. C₆₀ in water: Nanocrystal formation and microbial response. *Environ. Sci. Technol.* **2005**, *39*, 4307–4316. [[CrossRef](#)] [[PubMed](#)]
22. Sayes, C.M.; Fortner, J.D.; Guo, W.; Lyon, D.; Boyd, A.M.; Ausman, K.D.; Tao, Y.J.; Sitharaman, B.; Wilson, L.J.; Hughes, J.B.; et al. The differential cytotoxicity of water-soluble fullerenes. *Nano Lett.* **2004**, *4*, 1881–1887. [[CrossRef](#)]
23. Sayes, C.M.; Gobin, A.M.; Ausman, K.D.; Mendez, J.; West, J.L.; Colvin, V.L. Nano-C₆₀ cytotoxicity is due to lipid peroxidation. *Biomaterials* **2005**, *26*, 7587–7595. [[CrossRef](#)] [[PubMed](#)]
24. Oberdorster, G.; Oberdorster, E.; Oberdorster, J. Nanotoxicology: An emerging discipline evolving from studies of ultrafine particles. *Environ. Health Perspect.* **2005**, *113*, 823–839. [[CrossRef](#)]
25. Kraszewski, S.; Tarek, M.; Treptow, W.; Ramseyer, C. Affinity of C₆₀ Neat Fullerenes with Membrane Proteins: A Computational Study on Potassium Channels. *ACS Nano* **2010**, *4*, 4158–4164. [[CrossRef](#)]
26. Calvaresi, M.; Furini, S.; Domene, C.; Bottoni, A.; Zerbetto, F. Blocking the Passage: C₆₀ Geometrically Clogs K⁺ Channels. *ACS Nano* **2015**, *9*, 4827–4834. [[CrossRef](#)]
27. Marcorin, G.L.; Da Ros, T.; Castellano, S.; Stefanchich, G.; Bonin, I.; Miertus, S.; Prato, M. Design and synthesis of novel 60 fullerene derivatives as potential HIV aspartic protease inhibitors. *Org. Lett.* **2000**, *2*, 3955–3958. [[CrossRef](#)]
28. Strom, T.A.; Durdagi, S.; Ersoz, S.S.; Salmas, R.E.; Supuran, C.T.; Barron, A.R. Fullerene-based inhibitors of HIV-1 protease. *J. Pept. Sci.* **2015**, *21*, 862–870. [[CrossRef](#)]
29. Belgorodsky, B.; Fadeev, L.; Ittah, V.; Benyamini, H.; Zelner, S.; Huppert, D.; Kotlyar, A.B.; Gozin, M. Formation and characterization of stable human serum albumin-tris-malonic acid [C₆₀]fullerene complex. *Bioconjug. Chem.* **2005**, *16*, 1058–1062. [[CrossRef](#)]
30. Belgorodsky, B.; Fadeev, L.; Kolsenik, J.; Gozin, M. Formation of a soluble stable complex between pristine C₆₀-fullerene and a native blood protein. *ChemBiochem* **2006**, *7*, 1783–1789. [[CrossRef](#)]
31. Wu, H.; Lin, L.; Wang, P.; Jiang, S.; Dai, Z.; Zou, X. Solubilization of pristine fullerene by the unfolding mechanism of bovine serum albumin for cytotoxic application. *Chem. Commun.* **2011**, *47*, 10659–10661. [[CrossRef](#)] [[PubMed](#)]
32. Mashino, T.; Okuda, K.; Hirota, T.; Hirobe, M.; Nagano, T.; Mochizuki, M. Inhibitory effect of fullerene derivatives on glutathione reductase. *Fuller. Sci. Technol.* **2001**, *9*, 191–196. [[CrossRef](#)]
33. Iwata, N.; Mukai, T.; Yamakoshi, Y.N.; Hara, S.; Yanase, T.; Shoji, M.; Endo, T.; Miyata, N. Effects of C₆₀, a fullerene, on the activities of glutathione S-transferase and glutathione-related enzymes in rodent and human livers. *Fuller. Sci. Technol.* **1998**, *6*, 213–226. [[CrossRef](#)]
34. Marisa, I.; Asnicar, D.; Matozzo, V.; Martucci, A.; Finos, L.; Marin, M.G. Toxicological effects and bioaccumulation of fullerene C₆₀ (FC₆₀) in the marine bivalve *Ruditapes philippinarum*. *Ecotoxicol. Environ. Saf.* **2021**, *207*, 111560. [[CrossRef](#)]
35. Monticelli, L.; Barnoud, J.; Orłowski, A.; Vattulainen, I. Interaction of C₇₀ fullerene with the Kv1.2 potassium channel. *Phys. Chem. Chem. Phys.* **2012**, *14*, 12526–12533. [[CrossRef](#)]
36. Lee, O.-S.; Petrenko, V.I.; Siposova, K.; Musatov, A.; Park, H.; Lanceros-Mendez, S. How fullerenes inhibit the amyloid fibril formation of hen lysozyme. *J. Ind. Eng. Chem.* **2022**, *106*, 168–176. [[CrossRef](#)]
37. Zhu, Z.W.; Schuster, D.I.; Tuckerman, M.E. Molecular dynamics study of the connection between flap closing and binding of fullerene-based inhibitors of the HIV-1 protease. *Biochemistry* **2003**, *42*, 1326–1333. [[CrossRef](#)]
38. Kamat, J.P.; Devasagayam, T.P.A.; Priyadarsini, K.I.; Mohan, H. Reactive oxygen species mediated membrane damage induced by fullerene derivatives and its possible biological implications. *Toxicology* **2000**, *155*, 55–61. [[CrossRef](#)]
39. Dugan, L.L.; Gabrielsen, J.K.; Yu, S.P.; Lin, T.S.; Choi, D.W. Buckminsterfullerenol free radical scavengers reduce excitotoxic and apoptotic death of cultured cortical neurons. *Neurobiol. Dis.* **1996**, *3*, 129–135. [[CrossRef](#)]
40. Yang, L.-Y.; Gao, J.-L.; Gao, T.; Dong, P.; Ma, L.; Jiang, F.-L.; Liu, Y. Toxicity of polyhydroxylated fullerene to mitochondria. *J. Hazard. Mater.* **2016**, *301*, 119–126. [[CrossRef](#)]

41. Yamawaki, H.; Iwai, N. Cytotoxicity of water-soluble fullerene in vascular endothelial cells. *Am. J. Physiol.-Cell Physiol.* **2006**, *290*, C1495–C1502. [[CrossRef](#)] [[PubMed](#)]
42. Wang, T.; Duan, Y. Ligand Entry and Exit Pathways in the β_2 -Adrenergic Receptor. *J. Mol. Biol.* **2009**, *392*, 1102–1115. [[CrossRef](#)] [[PubMed](#)]
43. Frisch, M.J.T.; Trucks, G.W.; Schlegel, H.B.; Scuseria, G.E.; Robb, M.A.; Cheeseman, J.R.; Montgomery, J.A., Jr.; Vreven, T.; Kudin, K.N.; Burant, J.C.; et al. *Gaussian 03 Revision B.05*; Gaussian Inc.: Pittsburgh, PA, USA, 2004.
44. Bayly, C.I.; Cieplak, P.; Cornell, W.D.; Kollman, P.A. A well-behaved electrostatic potential based method using charge restraints for deriving atomic charges: The RESP model. *J. Phys. Chem.* **1993**, *97*, 10269–10280. [[CrossRef](#)]
45. Cezard, C.; Vanqueler, E.; Pecher, J.; Sonnet, P.; Cieplak, P.; Derat, E.; Dupradeau, F.-Y. COMP 267-RESP charge derivation and force field topology database generation for complex bio-molecular systems and analogs. In *Abstracts of Papers of the American Chemical Society*; American Chemical Society: Washington, DC, USA, 2008; Volume 236.
46. Cherezov, V.; Rosenbaum, D.M.; Hanson, M.A.; Rasmussen, S.G.F.; Thian, F.S.; Kobilka, T.S.; Choi, H.-J.; Kuhn, P.; Weis, W.I.; Kobilka, B.K.; et al. High-resolution crystal structure of an engineered human β_2 -adrenergic G protein-coupled receptor. *Science* **2007**, *318*, 1258–1265. [[CrossRef](#)]
47. Reiner, S.; Ambrosio, M.; Hoffmann, C.; Lohse, M.J. Differential Signaling of the Endogenous Agonists at the β_2 -Adrenergic Receptor. *J. Biol. Chem.* **2010**, *285*, 36188–36198. [[CrossRef](#)] [[PubMed](#)]
48. Kleinau, G.; Pratzka, J.; Nuernberg, D.; Grueters, A.; Fuehrer-Sakel, D.; Krude, H.; Koehrl, J.; Schoeneberg, T.; Biebermann, H. Differential Modulation of Beta-Adrenergic Receptor Signaling by Trace Amine-Associated Receptor 1 Agonists. *PLoS ONE* **2011**, *6*, e27073. [[CrossRef](#)]
49. Berendsen, H.J.C.; van der Spoel, D.; van Drunen, R. GROMACS: A message-passing parallel molecular dynamics implementation. *Comput. Phys. Commun.* **1995**, *91*, 43–56. [[CrossRef](#)]
50. Hess, B.; Bekker, H.; Berendsen, H.J.C.; Fraaije, J. LINCS: A linear constraint solver for molecular simulations. *J. Comput. Chem.* **1997**, *18*, 1463–1472. [[CrossRef](#)]
51. Berendsen, H.J.C.; Postma, J.P.M.; van Gunsteren, W.F.; DiNola, A.; Haak, J.R. Molecular dynamics with coupling to an external bath. *J. Chem. Phys.* **1984**, *81*, 3684–3690. [[CrossRef](#)]
52. Romo, T.D.; Grossfield, A.; Pitman, M.C. Concerted Interconversion between Ionic Lock Substates of the β_2 Adrenergic Receptor Revealed by Microsecond Timescale Molecular Dynamics. *Biophys. J.* **2010**, *98*, 76–84. [[CrossRef](#)]
53. Jaeschke, H.; Kleinau, G.; Sontheimer, J.; Mueller, S.; Krause, G.; Paschke, R. Preferences of transmembrane helices for cooperative amplification of $G_{\alpha s}$ and $G_{\alpha q}$ signaling of the thyrotropin receptor. *Cell. Mol. Life Sci.* **2008**, *65*, 4028–4038. [[CrossRef](#)] [[PubMed](#)]
54. Kofuku, Y.; Ueda, T.; Okude, J.; Shiraiishi, Y.; Kondo, K.; Maeda, M.; Tsujishita, H.; Shimada, I. Efficacy of the β_2 -adrenergic receptor is determined by conformational equilibrium in the transmembrane region. *Nat. Commun.* **2012**, *3*, 1045. [[CrossRef](#)]
55. Thevenin, D.; Roberts, M.F.; Lazarova, T.; Robinson, C.R. Identifying interactions between transmembrane helices from the adenosine A_2A receptor. *Biochemistry* **2005**, *44*, 16239–16245. [[CrossRef](#)] [[PubMed](#)]
56. Thevenin, D.; Lazarova, T. Stable interactions between the transmembrane domains of the adenosine A_2A receptor. *Protein Sci.* **2008**, *17*, 1188–1199. [[CrossRef](#)] [[PubMed](#)]